

Combining CPT-conjugate Neutrino channels at Fermilab

Andreas Jansson¹, Olga Mena², Stephen Parke¹ and Niki Saoulidou¹

¹ *Fermi National Accelerator Laboratory*

P.O.Box 500, Batavia, IL 60510, USA and

² *INFN Sez. di Roma, Dipartimento di Fisica, Università di Roma “La Sapienza”,*

P.le A. Moro, 5, I-00185 Roma, Italy

(Dated: November 2, 2018)

Abstract

We explore an alternative strategy to determine the neutrino mass hierarchy by making use of possible future neutrino facilities at Fermilab. Here, we use CPT-conjugate neutrino channels, exploiting a ν_μ beam from the NuMI beamline and a $\bar{\nu}_e$ beam from a betabeam experimental setup. Both experiments are performed at approximately the same $\langle E \rangle / L$. We present different possible accelerator scenarios for the betabeam neutrino setup and fluxes. This CPT-conjugate neutrino channel scenario can extract the neutrino mass hierarchy down to $\sin^2 2\theta_{13} \approx 0.02$.

PACS numbers: 14.60Pq

I. INTRODUCTION

During the last several years the physics of neutrinos has achieved remarkable progress. The experiments with solar [1, 2, 3, 4, 5, 6], atmospheric [7], reactor [8], and also long-baseline accelerator [9, 10, 11] neutrinos, have provided compelling evidence for the existence of neutrino oscillations, implying non zero neutrino masses. The present data require two large (θ_{12} and θ_{23}) and one small (θ_{13}) angles in the neutrino mixing matrix [12], and at least two mass squared differences, $\Delta m_{ji}^2 \equiv m_j^2 - m_i^2$ (where m_j 's are the neutrino masses), one driving the atmospheric (Δm_{31}^2) and the other one the solar (Δm_{21}^2) neutrino oscillations. The mixing angles θ_{12} and θ_{23} control the solar and the dominant atmospheric neutrino oscillations, while θ_{13} is the angle limited by the data from the CHOOZ and Palo Verde reactor experiments [13, 14].

The Super-Kamiokande (SK) [7] and K2K [9] data are well described in terms of dominant $\nu_\mu \rightarrow \nu_\tau$ ($\bar{\nu}_\mu \rightarrow \bar{\nu}_\tau$) vacuum oscillations. A recent global fit [15] provides the following 3σ allowed ranges for the atmospheric mixing parameters

$$|\Delta m_{31}^2| = (2 - 3.2) \times 10^{-3} \text{eV}^2, \quad 0.32 < \sin^2 \theta_{23} < 0.64. \quad (1)$$

The sign of Δm_{31}^2 , $\text{sign}(\Delta m_{31}^2)$, cannot be determined with the existing data. The two possibilities, $\Delta m_{31}^2 > 0$ or $\Delta m_{31}^2 < 0$, correspond to two different types of neutrino mass ordering: normal hierarchy and inverted hierarchy. In addition, information on the octant in which θ_{23} lies, if $\sin^2 2\theta_{23} \neq 1$, is beyond the reach of present experiments.

The 2-neutrino oscillation analysis of the solar neutrino data, including the results from the complete salt phase of the Sudbury Neutrino Observatory (SNO) experiment [6], in combination with the KamLAND spectrum data [16], shows that the solar neutrino oscillation parameters lie in the low-LMA (Large Mixing Angle) region, with best fit values [15] $\Delta m_{21}^2 = 7.9 \times 10^{-5} \text{eV}^2$ and $\sin^2 \theta_{12} = 0.30$.

A combined 3-neutrino oscillation analysis of the solar, atmospheric, reactor and long-baseline neutrino data [15] constrains the third mixing angle to be $\sin^2 \theta_{13} < 0.04$ at the 3σ C.L. However, the bound on $\sin^2 \theta_{13}$ is dependent on the precise value of Δm_{31}^2 .

The future goals for the study of neutrino properties is to precisely determine the already measured oscillation parameters and to obtain information on the unknown ones: namely θ_{13} , the CP-violating phase δ and the type of neutrino mass hierarchy (or equivalently

sign(Δm_{31}^2)). In the presence of matter effects, the neutrino (antineutrino) oscillation probability gets enhanced [17, 18] for the normal (inverted) hierarchy. Making use of the different matter effects for neutrinos and antineutrinos seems, in principle, the most promising way to distinguish among the two possibilities: normal versus inverted hierarchy. However, the sensitivity to the mass hierarchy determination from the neutrino-antineutrino comparison is highly dependent on the value of the CP violating phase. Thus, possible alternative methods were first proposed in Ref. [19]. In this paper we concentrate on the extraction of the neutrino mass hierarchy by combining a $\nu_\mu \rightarrow \nu_e$ experiment with its CPT conjugated channel $\bar{\nu}_e \rightarrow \bar{\nu}_\mu$, see Ref. [19]. More recently, it is primarily the CPT-conjugate channel pairs that give the CERN-MEMPHYS proposal sensitivity to the hierarchy, see Ref. [20]. If nature respects CPT symmetry, then, at the same E/L the only difference between the two flavor transitions can come from matter effects and that near the first oscillation maximum

$$P(\nu_\mu \rightarrow \nu_e) > P(\bar{\nu}_e \rightarrow \bar{\nu}_\mu) \quad \text{for Normal Hierarchy}$$

and $P(\nu_\mu \rightarrow \nu_e) < P(\bar{\nu}_e \rightarrow \bar{\nu}_\mu) \quad \text{for Inverted Hierarchy,}$

i.e. for the normal hierarchy the neutrino channel is enhanced and the antineutrino CPT conjugate channel suppressed and vice versa for the inverted hierarchy. This is the effect that will be exploited in this paper to determine the neutrino mass hierarchy.

We will show that the combination of the Phase I (neutrino-data only) of the long-baseline ν_e appearance experiment NO ν A [21], exploiting the off-axis technique¹ with a possible future betabeam facility [23, 24, 25, 26, 27] at Fermilab exploiting a $\bar{\nu}_e$ neutrino beam from radiative ion decays could help enormously in measuring the neutrino mass hierarchy. For our analysis, unless otherwise stated, we will use a representative value of $|\Delta m_{31}^2| = 2.5 \times 10^{-3} \text{ eV}^2$ and $\sin^2 2\theta_{23} = 1$. For the solar oscillation parameters Δm_{21}^2 and θ_{12} , we will use the best fit values quoted earlier in this section. The structure of the paper is as follows. In Section II we present the general physics strategy used to determine the neutrino mass

¹ A neutrino beam with narrow energy spectrum can be produced by placing the detector off-axis, i. e., at some angle with respect to the forward direction. The resulting neutrino spectrum is very narrow in energy (nearly monochromatic, $\Delta E/E \sim 15 - 25\%$) and peaked at lower energies with respect to the on-axis one. The off-axis technique allows a discrimination between the peaked ν_e oscillation signal and the intrinsic ν_e background which has a broad energy spectrum [22]. In addition, the off-axis technique reduces significantly the background resulting from neutral current interactions of higher energy neutrinos with a π^0 in the final state.

hierarchy including the CPT conjugate channels used in this paper. Section III contains a realistic description of possible future betabeam facilities at Fermilab. The different scenarios deal with different ions, baselines and luminosities, and the performance of the strategy followed here in each of these scenarios is illustrated in Section IV. The sensitivity curves for the several scenarios will be presented in Section V and the final remarks are summarized in Section VI. In the Appendix A, we discuss the details associated with comparing CPT conjugate neutrino oscillation probabilities.

II. COMBINING NEUTRINO CHANNELS

The strategy we have introduced in the previous section and we explain in detail here is different from the usual one, which exploits the combination of the neutrino and antineutrino oscillation channels. Typically, the proposed long baseline neutrino oscillation experiments have a single far detector and plan to run with the beam in two different modes, muon neutrinos and muon antineutrinos. In principle, by measuring the probability of neutrino and antineutrino flavor conversion, the values of the CP-violating phase δ and the $\text{sign}(\Delta m_{31}^2)$ could be extracted, since, in the presence of matter effects there will be two allowed regions for each type of hierarchy, normal or inverted, in the $P(\nu_\mu \rightarrow \nu_e)$ versus $P(\bar{\nu}_\mu \rightarrow \bar{\nu}_e)$ plane. In practice, the neutrino-antineutrino comparison does not provide the ideal tool to extract the neutrino mass hierarchy, as we explain below.

Suppose we compute the oscillation probabilities $P(\nu_\mu \rightarrow \nu_e)$ and $P(\bar{\nu}_\mu \rightarrow \bar{\nu}_e)$ for a given set of oscillation parameters and the CP-phase δ is varied between 0 and 2π : we obtain a closed CP trajectory (an ellipse) in the bi-probability space of neutrino and antineutrino conversion [28]. Matter effects are responsible for the departure of the center of the ellipses from the diagonal line in the bi-probability plane for normal and inverted hierarchy. In Figure 1, we have illustrated the case for $E = 2.0$ GeV and $L = 810$ km, which roughly correspond to those of the NO ν A experiment [21]. The distance between the center of the ellipse for the normal hierarchy (lower blue) and that for the inverted hierarchy (upper red) is governed by the size of the matter effects. Notice that the ellipses overlap for a significant fraction of values of the CP-phase δ for every allowed value of $\sin^2 2\theta_{13}$. This makes the determination of $\text{sign}(\Delta m_{31}^2)$ extremely difficult, i. e., the $\text{sign}(\Delta m_{31}^2)$ -extraction is not free of degeneracies.

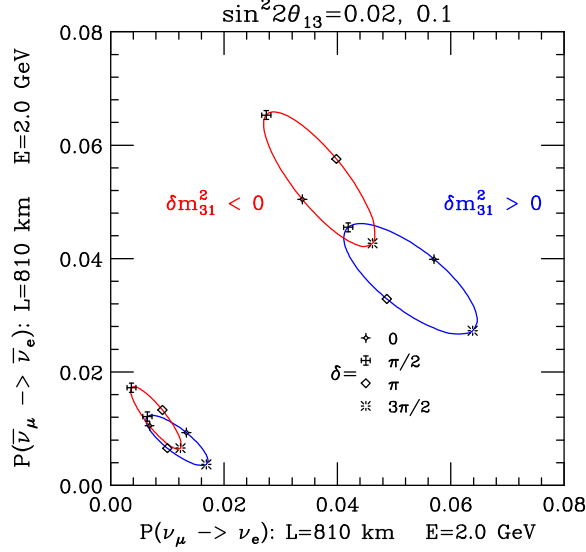


FIG. 1: The bi-probability plot for $P(\nu_\mu \rightarrow \nu_e)$ versus $P(\bar{\nu}_\mu \rightarrow \bar{\nu}_e)$ at a baseline of 810 km and an energy of 2.0 GeV for the normal (blue) and the inverted (red) hierarchies. The smaller, lower (larger, upper) ellipses are for $\sin^2 2\theta_{13} = 0.02$ (0.10).

Following the line of thought developed by Minakata, Nunokawa and Parke [19], we exploited in a previous work [29, 30] the neutrino data only from two experiments at different distances and at different off-axis locations, such that the $\langle E \rangle / L$ is the same for the two experiments (see also Refs. [31, 32, 33, 34, 35]). In the case of bi-probability plots for neutrino-neutrino modes at different distances (which will be referred as near (N) and far (F)), the CP-trajectory is also elliptical. In Figure 2 (a) we present the bi-probability plot for the mean energies and baselines of the ν_e appearance experiments T2K [36] and NO ν A [21]. The overlap of the two ellipses, which implies the presence of a degeneracy of the type of hierarchy with other parameters, is determined by their width and the difference in the slopes. Using the fact that matter effects are small ($aL \ll \Delta_{31}$, being $a = G_F N_e / \sqrt{2} \approx (4000 \text{ km})^{-1}$ the matter parameter), we can perform a perturbative expansion and assuming that the $\langle E \rangle / L$ of the near and far experiments is the same², at first order, the ratio of the slopes reads [19]

$$\frac{\alpha_+}{\alpha_-} \simeq 1 + 4(a_N L_N - a_F L_F) \left(\frac{1}{\Delta_{31}} - \frac{1}{\tan(\Delta_{31})} \right), \quad (2)$$

² The reason for this choice of $\langle E \rangle / L$ is explained in the next paragraph.

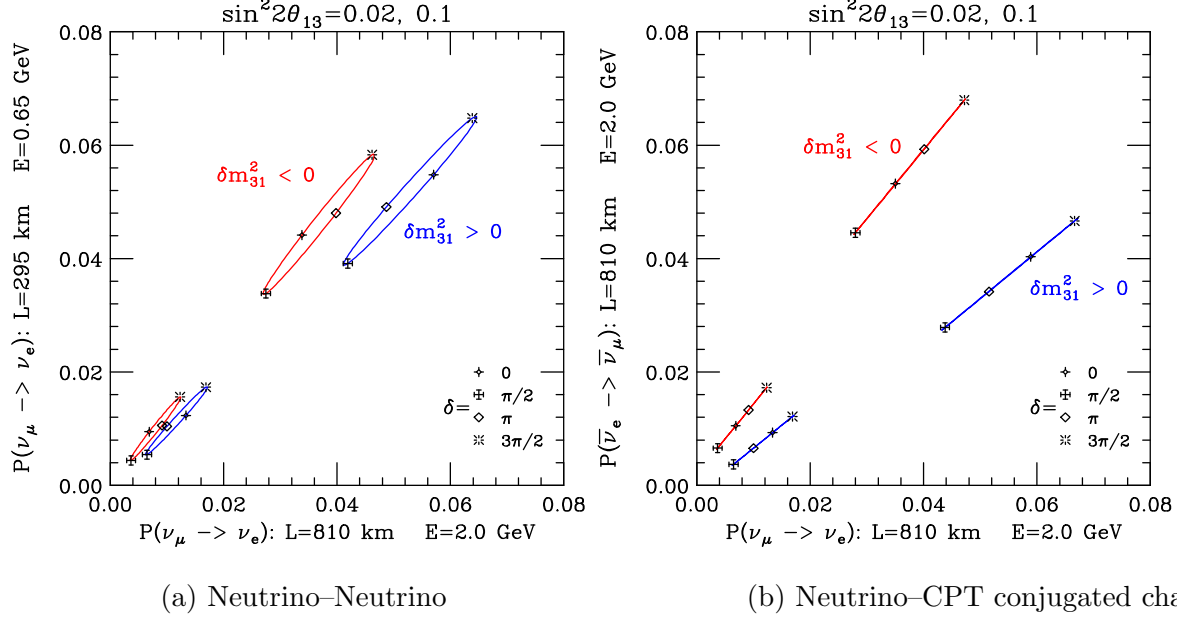


FIG. 2: (a) The left panel is the bi-probability plot for $P(\nu_\mu \rightarrow \nu_e)$ versus $P(\nu_\mu \rightarrow \nu_e)$ with baselines 295 km and 810 km for the normal (blue) and the inverted (red) hierarchies. The smaller, lower (larger, upper) ellipses are for $\sin^2 2\theta_{13} = 0.02$ (0.10). The mean neutrino energies are chosen such that the $\langle E \rangle/L$ for the two experiments are approximately identical.

(b) The right panel is the bi-probability plot for $P(\nu_\mu \rightarrow \nu_e)$ versus $P(\bar{\nu}_e \rightarrow \bar{\nu}_\mu)$ for the normal (blue) and the inverted (red) hierarchies. The baseline and mean neutrino energy for both experiments are 810 km and ~ 2 GeV, respectively. The smaller, lower (larger, upper) squashed ellipses are for $\sin^2 2\theta_{13} = 0.02$ (0.10).

where α_+ and α_- are the slopes of the center of the ellipses as one varies θ_{13} for normal and inverted hierarchies, a_F and a_N are the matter parameters, and L_F and L_N are the baselines for the two experiments. The separation between the center of the ellipses for the two hierarchies increases as the difference in the matter parameter times the path length, (aL) , for the two experiments increases. Also, since $(\Delta^{-1} - \cot \Delta)$ is a monotonically increasing function of Δ , we conclude that the smaller the energy, the larger the ratio of slopes, assuming the same $\langle E \rangle/L$. However the width of the ellipses is crucial: even when the separation between the central axes of the two regions is substantial, if the ellipses for the normal and inverted hierarchy overlap, the hierarchy cannot be resolved for values of the CP phase, δ , for which there is overlap. The width of the ellipses is determined by the difference in the $\langle E \rangle/L$ of the two experiments.

In the case of bi-probability plots for the $\nu_\mu \rightarrow \nu_e$ and its CPT conjugated channel $\bar{\nu}_e \rightarrow \bar{\nu}_\mu$ at the same energy divided by baseline, $\langle E \rangle / L$, the CPT-trajectory collapses to a line (see Figure 2 (b)). As for the neutrino-neutrino case, we can perform a perturbative expansion, and, assuming that the $\langle E \rangle / L$ of the CPT conjugated channels is the same (to minimize the ellipses width), at first order, the ratio of the slopes reads (see Appendix and also Ref. [19])

$$\frac{\alpha_+}{\alpha_-} \simeq 1 + 4(aL + a_{\text{CPT}}L_{\text{CPT}}) \left(\frac{1}{\Delta_{31}} - \frac{1}{\tan(\Delta_{31})} \right), \quad (3)$$

where α_+ and α_- are the slopes of the center of the ellipses as one varies θ_{13} for normal and inverted hierarchies, a and a_{CPT} are the matter parameters and L and L_{CPT} are the baselines for the two experiments which exploit the $\nu_\mu \rightarrow \nu_e$ and its CPT conjugated channel ($\bar{\nu}_e \rightarrow \bar{\nu}_\mu$). Notice that, compared to the neutrino-neutrino case given by Eq. (2), the separation between the center of the ellipses for the two hierarchies increases as the sum of the matter parameter times the baseline, aL , for both experiments does. Here the ratio of the slopes is enhanced by matter effects for both $\nu_\mu \rightarrow \nu_e$ and its CPT conjugated channel $\bar{\nu}_e \rightarrow \bar{\nu}_\mu$. Figure 2 (b) shows the bi-probability curves for the combination of these two flavor transitions, assuming that the two experiments are performed at the same mean energy and baseline. If the $\langle E \rangle / L$ of both experiments is the same, the ellipses will become lines with a negligible width. The separation of the lines for the normal and inverted hierarchy grows as the matter effects for both experiments increase. Consequently, the comparison of CPT conjugated channels is more sensitive to the neutrino mass hierarchy than the neutrino-neutrino one.

III. BETA BEAMS AT FERMILAB

A betabeam facility exploits a beam of electron neutrinos (antineutrinos) from boosted-ion β^+ (β^-) decays in the straight section of a storage ring [23, 24]. The idea of considering higher γ factors (and, consequently, longer detector baselines) was first proposed in Ref. [25]. An extensive phenomenological work has been devoted in order to optimize the betabeam physics reach, analyzing several scenarios with different γ factors, boosted-ions and/or detector baselines [26].

Early on, ^6He and ^{18}Ne were identified as optimal ions, because of the low Q factor of

their decay. The lower the neutrino energy is in the rest frame, the more boost is needed to get to a given energy, and since the angular spread of the beam goes as $1/\gamma$ this yields a more focused neutrino beam, which in turn produces more events in the far detector. Recently, it was proposed to use ^8Li and ^8B , which could potentially be produced in large amounts using a small storage ring with an internal gas target[38]. Since these ions have larger Q factor, they produce fewer neutrinos per ion in the far detector for a fixed neutrino energy and baseline. However, because less boost is needed, a smaller accelerator would be needed to achieve the same neutrino energy, as compared to the case of ^6He and ^{18}Ne . In this section we present possible betabeam scenarios at Fermilab, exploiting its current accelerator facilities. Since the analysis considered in this paper only requires anti-neutrinos from a beta-beam, we concentrate on ^6He and ^8Li .

A rather thorough study of achievable ion intensities has been done at CERN [37]. The CERN scenario uses the existing PS and SPS accelerators, and would in addition require a proton source (e.g. the proposed Superconducting Proton Linac), target station, ion source, ion linac and Rapid Cycling Synchrotron (RCS), as well as a decay ring operating at SPS top energy. Based on a ^6He ion production rate of $2 \times 10^{13}/\text{s}$, ions decaying in the straight section directed towards the experiment would produce approximately 3×10^{18} antineutrinos per year. We consider two possible scenarios at Fermilab, namely: 1) accelerating ^6He to Tevatron top energy and 2) accelerating ^8Li to Main Injector (MI) top energy. These two scenarios produce neutrinos of comparable energies. The ions would be generated using a proton source (e.g. the Project X linac) and accelerated using e.g. a linac and a small RCS before being injected into the existing Booster. Possibly, the Recycler could also be used to accumulate bunches while the MI is ramping. In both cases, a new decay ring would be needed to store the ions ³.

Extrapolating from the work done at CERN, it appears reasonable to expect a useful ion decay rate (decays in the direction of the experiment) of about 1×10^{18} ^6He per year in the Tevatron case. At this intensity, the average power deposition in the Tevatron would be about 1 W/m, which is a generally accepted limit for hands-on-maintenance. Preliminary simulations indicate that the Tevatron magnets would be able to handle the distributed energy deposition from decay products in the arcs, but special care would have to be taken

³ Note that if the Tevatron top energy is used (^6He), the decay ring would be very large and expensive.

to cope with the build-up of decay products in the straight sections. In the case of ^8Li in MI, the injectors could operate with a significantly higher duty factor, since there is no need to wait for the slow Tevatron ramp. However, at repetition rates and intensities corresponding to a useful ion decay rate of about 1×10^{19} per year, activation of the Booster from decay products would become a serious issue.

A very important property of the neutrino beam is the duty factor, defined as the relative fraction of time occupied by the neutrino pulse. This is used to suppress background by gating the data acquisition in the experiment. In the CERN study, a duty factor of a few per mil was obtained with considerable difficulty. A small duty factor is challenging because it requires the ions to be concentrated in very few bunches, which among other things can cause space-charge problems, in particular at low energies. Using the CERN number of 1×10^{12} ions per RCS cycle, and a Booster injection energy of around 500 MeV/u, the beam must be distributed over about 10 bunches in the Booster to keep the space charge tune shift at an acceptable level. Approximately eight transfers from the booster per MI cycle would be required to obtain 1×10^{19} useful ^8Li decays per year at MI top energy. Without RF manipulations, this would yield a neutrino beam duty factor of about 10%, but a duty factor of order 1% could likely be obtained by coalescing bunches at MI top energy⁴. In the case of ^6He , about twenty booster injections per cycle would be required per cycle, in order to compensate for the long Tevatron cycle and obtain a useful ^6He decay rate of 1×10^{18} per year. Assuming bunches are coalesced in the MI, this should also yield a neutrino beam duty factor of about 1%. Space charge is not expected to be an issue in the MI or Tevatron at these bunch intensities.

For the ^6He case, therefore, it appears possible to generate 10^{18} useful ion decays per year with a maximum gamma of $\gamma_{\text{He}} = 350$. For the ^8Li case, at a maximal gamma of $\gamma_{\text{Li}} = 55$, the rate could be higher (as explained above). We will explore an optimistic scenario of 5×10^{19} useful ion decays per year, as well a more pessimistic scenario of 10^{19} useful ion decays per year from ^8Li decays. We will assume a duty factor of 1% for both ion species. Table I shows the maximum Lorentz gamma factors in the Fermilab machines for the ^6He and ^8Li , as well as other ions considered in the literature.

⁴ Although coalescing is standard procedure for generating single proton bunches from 53 MHz booster beam, the stability of the coalescing process needs to be demonstrated when generating multiple intense coalesced bunches simultaneously.

Machine	${}^6\text{He}^{2+}$	${}^8\text{Li}^{3+}$	${}^{18}\text{Ne}^{10+}$	${}^8\text{B}^{5+}$
Linac	1.6	1.07	1.15	1.19
Booster	3.3	3.7	5.4	6.1
Main Injector	54	60	90	101
Tevatron	351	395	586	659

TABLE I: *Maximum Lorentz gamma factors obtainable in the Fermilab machines for different ions of interest.*

IV. POSSIBLE EXPERIMENTAL SETUPS AT FERMILAB

As we discussed in Section II, the most sensitive, degeneracy free method, to extract the neutrino mass hierarchy exploiting a future high intensity conventional neutrino beam ($\nu_\mu \rightarrow \nu_e$) is the combination of this channel with its CPT conjugate $\bar{\nu}_e \rightarrow \bar{\nu}_\mu$. Future facilities like betabeams (neutrino factories) can produce neutrino beams which are entirely (partially) composed of ν_e or $\bar{\nu}_e$.

The experimental strategy that we follow here is to combine the NO ν A experiment, which will measure the flavor transitions $\nu_\mu \rightarrow \nu_e$, with its CPT conjugated channel. The NO ν A experiment is expected to run at least five years with neutrinos. A 30 kton low density tracking calorimeter with an efficiency of 24% would be located at a baseline of 810 km and at 12 km off-axis distance from the beam center, resulting in a mean muon neutrino energy of 2.0 GeV. For the CPT conjugate channel, $\bar{\nu}_e \rightarrow \bar{\nu}_\mu$, we exploit possible, future betabeam facilities at Fermilab described in the previous section for two antineutrino emitters: ${}^6\text{He}$ and ${}^8\text{Li}$. A future neutrino factory exploiting neutrino fluxes from muon decays could also provide the $\bar{\nu}_e$ CPT conjugate channel, if μ^- 's are stored in the decay ring. In the present study we do not explore this possibility. For the ${}^6\text{He}$ ion case, (maximum $\gamma_{\text{He}} = 350$), the mean electron antineutrino energy is ~ 1.2 GeV ($\langle E_\nu \rangle \simeq \gamma_{\text{He}} E_{0,\text{He}}$, $E_{0,\text{He}} = 3.5 + m_e$ MeV, being the electron end-point energy for ${}^6\text{He}$). We present the results for two possible experimental ${}^6\text{He}$ setups. In the first scenario, we consider a single baseline $L = 810$ km, at which the NO ν A detector would be located, with a total detector mass of 40 kton. This first scenario could be easily achieved adding to the 30 kton NO ν A far detector a second 10 kton detector at the NO ν A far site. Possible detector technologies are Liquid Argon or iron calorimeter

detectors. Liquid Argon (LAr) detectors have excellent efficiency, background rejection and energy resolution, but they could suffer from a large atmospheric neutrino background, which could be overcome only if the beam duty cycle is $< 10^{-4}$ [24]. In the second scenario, we consider a detector similar to the one of the MINOS [10] experiment (5 kton) at 735 km but twice in size. If the ion luminosity could be improved by a factor of two, MINOS far detector would be sufficient. This scenario benefits from the lower atmospheric neutrino backgrounds at the MINOS site. The beam duty cycle would not, therefore, be a major issue, and a duty factor of $\sim 1\%$ would be sufficient to overcome the atmospheric neutrino background in this case. For the ${}^8\text{Li}$ ion case, (maximum $\gamma_{\text{Li}} = 50$), the mean electron antineutrino energy is ~ 1.8 GeV ($\langle E_\nu \rangle \simeq \gamma_{\text{Li}} E_{0,\text{Li}}$, $E_{0,\text{Li}} = 16$ MeV, being the electron end-point energy for ${}^8\text{Li}$). In order to ensure an almost degeneracy free hierarchy measurement, the $\langle E \rangle / L$ of the $\nu_\mu \rightarrow \nu_e$ channel from NO ν A and its CPT conjugate channel should be similar, therefore the detector should be located at $L = 300$ km. We will consider 5×10^{19} (1×10^{19}) useful ion decays per year with a 10 (50) kton detector respectively. As previously discussed, considering 5×10^{19} useful ion decays is a quite optimistic assumption. However, notice that the same statistics could be achieved with the more conservative assumption of 1×10^{19} useful ion decays per year, with a larger 50 kton detector (these two configurations provide the same statistics). Due to the lower neutrino energies, the detector could be a Liquid Argon TPC, a NO ν A-like Totally Active Scintillator Detector (TASD), or a water Cherenkov. For the NUMI off-axis neutrino beam, we have not considered a binning in the signal, since neutrino events will lie in a very narrow energy window [1.5,2.5] GeV. The ${}^6\text{He}$ and ${}^8\text{Li}$ antineutrino betabeams have been divided in three energy bins, assuming an energy detection threshold of 0.5 GeV. For the ${}^6\text{He}$ case, we divide the signal in three energy bins, in the energy ranges [0.5,1.0], [1.0,1.5] and [1.5,2.4] GeV, respectively. In the ${}^8\text{Li}$ case, the energy ranges are [0.5,0.75], [0.75,1.0] and [1.0,1.5] GeV, respectively.

Figure 3 depict the bi-event plots for the combination of the NO ν A neutrino events ($\nu_\mu \rightarrow \nu_e$) with its CPT conjugated channel ($\bar{\nu}_e \rightarrow \bar{\nu}_\mu$) from the betabeam experiment, resulting from the decays of ${}^6\text{He}$ (left panel) and ${}^8\text{Li}$ (right panel), for both normal and inverted hierarchies. The statistics considered for NO ν A correspond to Phase I of the experiment (neutrino running only). For the ${}^6\text{He}$ betabeam experiment, we assume a number of useful ion decays of 10^{18} per year, five years of data taking, and a 40 kton detector located at 810 km. For the ${}^8\text{Li}$ betabeam experiment, we assume 5×10^{19} (1×10^{19}) useful ion decays

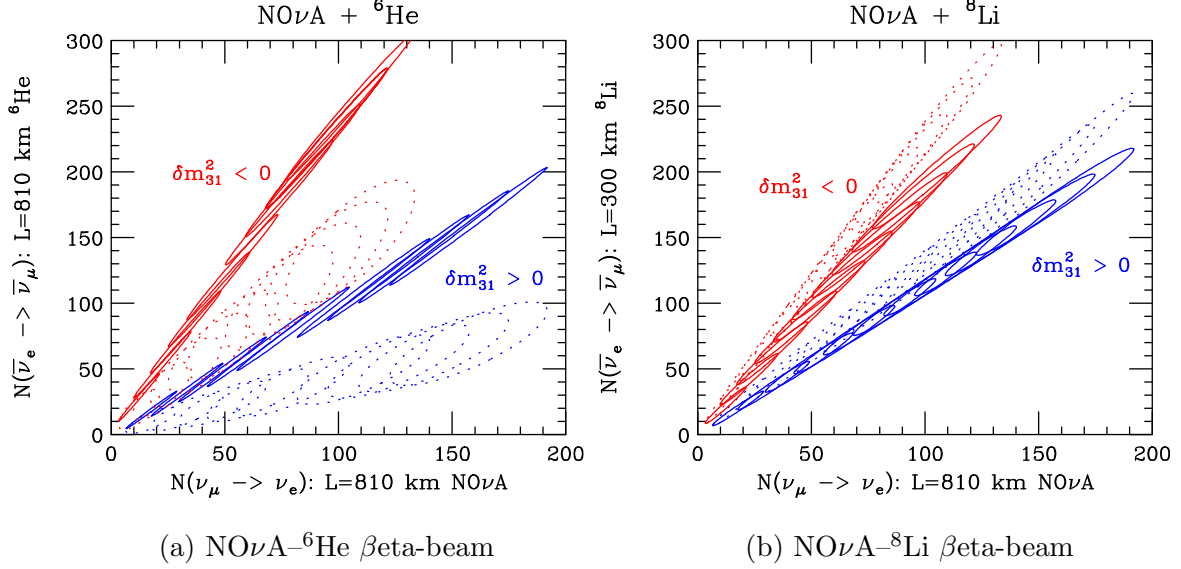


FIG. 3: (a) The allowed regions in the bi-event plot for $N(\nu_\mu \rightarrow \nu_e)$ for NOνA versus $N(\bar{\nu}_e \rightarrow \bar{\nu}_\mu)$ for a betabeam experiment which exploits antineutrinos from ${}^6\text{He}$ decays with $\gamma_{\text{He}} = 350$, and a detector of 40 kton located at a distance of $L = 810$ km. The blue (red) ellipses denote normal (inverted) hierarchies. From bottom up, the ellipses correspond to $\sin^2 2\theta_{13}$ varying from 0.01 to 0.1. The solid (dashed) ellipses illustrate the third (second) energy bins of the betabeam spectrum. (b) Same as (a) but with antineutrino fluxes resulting from ${}^8\text{Li}$ decays, and a detector of 10 kton at 300 km.

per year, ten years of data taking, and a 10 (50) kton detector located at 300 km.

Figure 3 (a) shows that, for the combination of NOνA off-axis neutrino events with the antineutrino events from ${}^6\text{He}$ decays, the separation between the bi-event contours for the normal and inverted hierarchies is larger than in the case of ${}^8\text{Li}$ generated antineutrino events, as seen in Figure 3 (b). As previously explained, the difference in the slopes of the two hierarchies is proportional to the sum of the size of matter effects times the baseline, $a_{\text{NO}\nu\text{A}}L_{\text{NO}\nu\text{A}} + a_{\text{CPT}}L_{\text{CPT}}$. The product $a_{\text{CPT}}L_{\text{CPT}}$ is larger for the ${}^6\text{He}$ betabeam $\bar{\nu}_e$ events (with a baseline of 810 km), than for the ${}^8\text{Li}$ betabeam $\bar{\nu}_e$ events (with a baseline of 300 km). The solid (dashed) contours in Figure 3 show the number of betabeam antineutrino events in the second (third) energy bin. When the $\langle E \rangle / L$ of the $\nu_\mu \rightarrow \nu_e$ and its CPT conjugated channel are similar, the ellipses width is minimal (they collapse to a line) and therefore the elliptical contours for the normal and inverted hierarchies will not overlap, regardless the value of the CP violating phase δ . For the combination of NOνA off-axis neutrino events

with the ${}^6\text{He}$ betabeam antineutrino events, there exists a clear difference between the second and third energy bins in the bi-event contours: while they are ellipses in the former, they are almost lines in the latter. Only in the third energy bin ($[1.5, 2.5]$ GeV) is the $\langle E \rangle / L$ the same for the ${}^6\text{He}$ betabeam $\bar{\nu}_e$ and for the NO ν A ν_μ events. For the ${}^8\text{Li}$ case the ellipses width is minimal for both the second and third energy bins, since both bins are close to $E \sim 0.8$ GeV, the energy at which the $(\langle E \rangle / L)_{Li}$ equals the $(\langle E \rangle / L)_{NO\nu A}$.

V. SIGN Δm_{31}^2 SENSITIVITIES

In this section we present the physics results from the combination of antineutrino data, resulting from several possible betabeam setups, with the NO ν A neutrino data.

Figure 4 (a) shows the 90% C.L mass hierarchy sensitivity, assuming two degrees of freedom statistics (2 d.o.f, that is, $\Delta\chi^2 > 4.21$) for the combination of NO ν A neutrino data with the ${}^6\text{He}$ betabeam antineutrino data, neglecting the background in the $\bar{\nu}_e \rightarrow \bar{\nu}_\mu$ channel. In order to safely neglect the atmospheric neutrino background, one would need a very small, experimentally challenging duty factor for the betabeam neutrino fluxes. The baseline for the two experiments is fixed at 810 km and the $\gamma_{\text{He}} = 350$, in order to have a similar $\langle E \rangle / L$ in both the muon neutrino and the electron antineutrino channels. The binning of the signal has been chosen as quoted in the previous section. We have considered a flux of 10^{18} antineutrinos per year, and five years of data taking. The blue (red) lines assume normal (inverted) hierarchy, and the solid (dotted) lines depict the results for a betabeam antineutrino experiment with a 40 (10) kton detector. For the 40 kton detector, the sensitivity is better for the inverted mass hierarchy, since in this case statistics is dominated by the antineutrino channel $\bar{\nu}_e \rightarrow \bar{\nu}_\mu$. For the 10 kton detector, the two channels (i.e., the neutrino channel from NO ν A and the antineutrino channel from the betabeam experiment) will have similar statistics and therefore the sensitivity for the normal and the inverted mass hierarchies are similar. As a comparison, we also show the results for the NO ν A experiment (upgraded by a factor of five in statistics), assuming five years of neutrino and five years of antineutrino data taking, see the dashed curves in Figure 4. The setup proposed here improves the sensitivity of the NO ν A upgraded experiment by an order of magnitude, and more importantly, eliminates the dependence of the mass hierarchy determination on the value of the CP violating phase δ .

Figure 4 (b) shows the 90% C.L mass hierarchy sensitivity, assuming two degrees of freedom statistics (2 d.o.f, that is, $\Delta\chi^2 > 4.21$) for the combination of NO ν A neutrino data with the ${}^6\text{Li}$ betabeam antineutrino data, neglecting the background in the $\bar{\nu}_e \rightarrow \bar{\nu}_\mu$ channel. The baseline for the betabeam experiment is $L = 300$ km and the binning of the signal has been chosen as described in the previous section. We assume 5×10^{19} ${}^8\text{Li}$ generated antineutrinos per year, and ten years of data taking. The blue (red) lines assume normal (inverted) hierarchy, and the solid (dotted) lines depict the results for a betabeam antineutrino experiment with a 10 (2) kton detector. For the case of ${}^8\text{Li}$ betabeam experiment, the sensitivity is similar for the normal and inverted mass hierarchy, and smaller than in the case of ${}^6\text{He}$ betabeam experiment. This is expected, since at a shorter baseline (300 km) the product of the matter potential times the distance is reduced. Again, the combination of the NO ν A neutrino data only with the ${}^8\text{Li}$ betabeam antineutrino data provides a much better sensitivity to the mass hierarchy than the NO ν A upgraded experiment alone.

However, as previously stated, the beam duty cycle needed in order to neglect the atmospheric neutrino background is highly challenging. For a MINOS-like detector, there are 30 atmospheric neutrino interactions per kton-year which could mimic a muon coming from the oscillated $\bar{\nu}_e \rightarrow \bar{\nu}_\mu$ [39]. In order to avoid such a large background, we have assumed a betabeam duty cycle $\sim 10^{-2}$, which seems experimentally achievable. Figure 5 shows the equivalent to Figure 4 when adding the atmospheric neutrino background quoted above, rescaled accordingly to the detector sizes and the exposure times. Notice that the presence of a non negligible atmospheric neutrino background in the antineutrino channel $\bar{\nu}_e \rightarrow \bar{\nu}_\mu$ reduces the sensitivity reach especially for the case of the inverted mass hierarchy. However, even in the presence of a non negligible background, and with the very conservative assumption of a 10^{-2} beam duty cycle, the combination of the betabeam antineutrino data with the NO ν A Phase I neutrino data, provides better sensitivity than the NO ν A experiment alone (upgraded by a factor of five and running in both neutrino and antineutrino mode). If a smaller duty factor $< 10^{-2}$ could be achievable (as commonly assumed, following Ref. [24]) the sensitivity to the mass hierarchy would lie within the limits illustrated in Figure 4 (the most optimistic case with no atmospheric neutrino induced background) and the limits depicted in Figure 5 (the most pessimistic case with atmospheric neutrino backgrounds and a beam duty cycle $\sim 10^{-2}$).

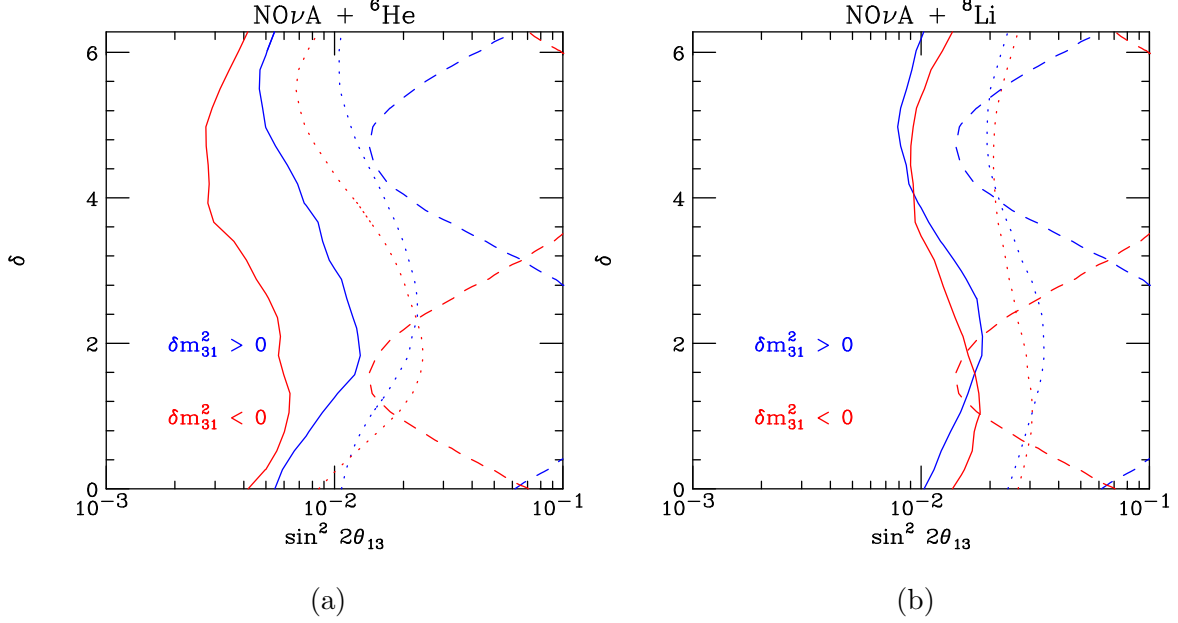


FIG. 4: (a) The 90% CL (2 d.o.f.) hierarchy resolution curves for different exposures for the ${}^6\text{He}$ betabeam $\bar{\nu}_e$ fluxes at 810 km, combined with five years of neutrino data only from the NO ν A far detector, located 12 km off-axis at 810 km. Only backgrounds in the NO ν A experiment have been included. The blue (red) curves assume normal (inverted) hierarchy. The solid (dotted) line depicts the results for 2×10^{20} (5×10^{19}) useful ion decays times kton. The blue (red) dashed curve shows the sensitivity reach at 90% CL (2 d.o.f.) from the combination of neutrino and antineutrino data from the NO ν A experiment, assuming five years running in both neutrinos and antineutrinos with a factor of five increase in statistics and normal (inverted) hierarchy. (b) The 90% CL (2 d.o.f.) hierarchy resolution curves for different exposures for the ${}^8\text{Li}$ betabeam electron antineutrino fluxes at 300 km, combined with muon neutrino data only from the NO ν A far detector at 12 km off-axis at 810 km. Again, only backgrounds in the NO ν A experiment have been included. The blue (red) curves assume normal (inverted) hierarchy. The solid (dotted) line depicts the results for 5×10^{21} (10^{21}) useful ion decays times kton.

VI. CONCLUSIONS

We have explored an alternative strategy for measuring the neutrino mass hierarchy. Unlike the approach followed by future long baseline neutrino oscillation experiments that combine the neutrino–antineutrino data, the combination of the CPT conjugated channels that we study here provides an almost degeneracy free determination of the neutrino mass hi-

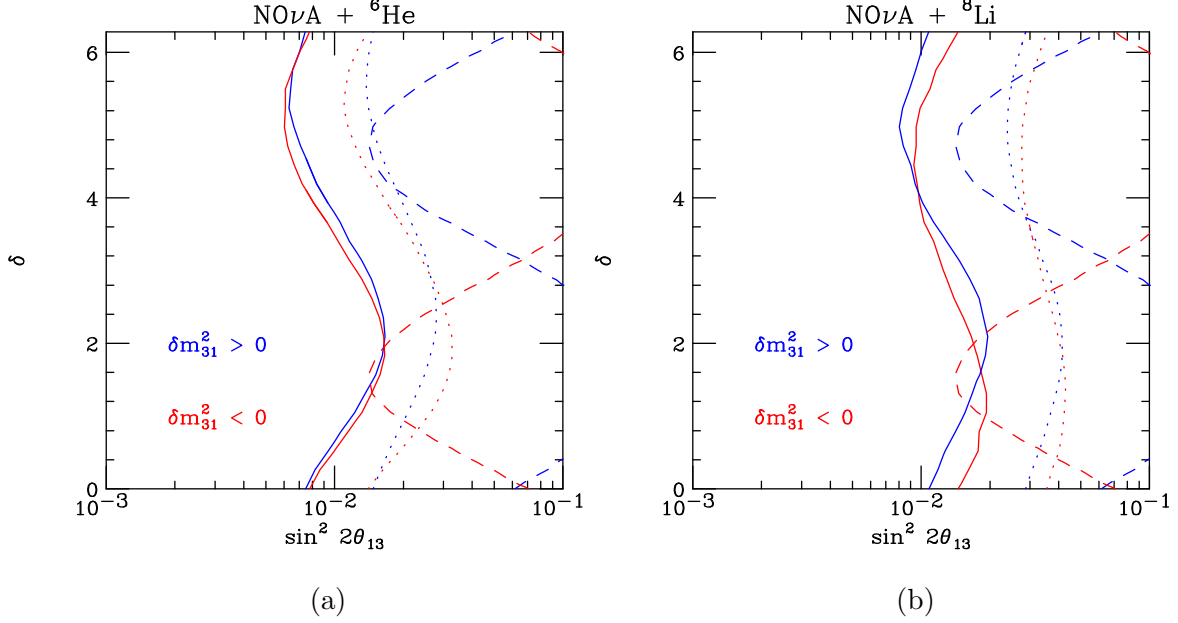


FIG. 5: Same as Figs. 4 but including backgrounds in the betabeam electron antineutrino data, see text for details.

erarchy, provided the two channels have similar $\langle E \rangle / L$. Future neutrino facilities at Fermilab could provide these CPT neutrino-conjugated channels. The NOνA ν_e off-axis appearance experiment could provide the $\nu_\mu \rightarrow \nu_e$ channel. A future betabeam facility based at Fermilab could provide the CPT-conjugated $\bar{\nu}_e \rightarrow \bar{\nu}_\mu$ channel. A realistic estimate of the expected electron antineutrino fluxes from boosted ion decays is presented. We propose two possible accelerator scenarios for generating the betabeam electron antineutrino fluxes: the Tevatron, which could accelerate ${}^6\text{He}$ ions, and the Main Injector, which could accelerate ${}^8\text{Li}$ ions. In the case of the Tevatron, the decay ring would be very large and possibly prohibitively expensive. The first scenario could benefit from the NOνA far detector at $L = 810$ km, (but the decay ring needed would be very large) ; for the second scenario, an additional, although smaller 2 – 10 kton MINOS like detector at a shorter baseline, $L = 300$ km, would be necessary (the decay ring needed in this case would be smaller, though). In the more pessimistic case, with a modest beam duty cycle of 10^{-2} and including realistic atmospheric neutrino backgrounds, the neutrino mass hierarchy could be determined for $\sin^2 2\theta_{13} > 0.01$, independently of the value of the CP violating phase δ , for both accelerator possibilities. These two alternative choices could improved by an order of magnitude the sensitivity to the neutrino mass hierarchy obtained by a future NOνA upgraded experiment exploiting

both neutrinos and antineutrinos.

Acknowledgments

We wish to thank A. Donini for useful comments on the manuscript. OM is supported by the European Programme “The Quest for Unification” contract MRTN-CT-2004-503369. Fermilab is operated by FRA under DOE contract DE-AC02-07CH11359. OM would like to thank the Theoretical Physics Department at Fermilab for hospitality and support.

APPENDIX A: CPT CONJUGATE PROBABILITIES:

The amplitudes for $\nu_\mu \rightarrow \nu_e$ and $\bar{\nu}_e \rightarrow \bar{\nu}_\mu$ consists of two terms, one associated with the atmospheric δm^2 scale and the other associated with the solar δm^2 scale. Thus, the probability for these the CPT-conjugate processes contain three terms; the square of each of the amplitudes plus the interference term between the two amplitudes which depends on the CP phase δ . For the normal (upper sign) and inverted (lower sign) hierarchy, the $\nu_\mu \rightarrow \nu_e$ and $\bar{\nu}_e \rightarrow \bar{\nu}_\mu$ appearance probabilities are given by

$$\begin{aligned} P(\nu_\mu \rightarrow \nu_e) &= X_\pm \theta^2 \pm 2\sqrt{X_\pm} \sqrt{P_\odot} \theta \cos(\pm\Delta_{31} + \delta) + P_\odot \\ \bar{P}(\bar{\nu}_e \rightarrow \bar{\nu}_\mu) &= X_\mp \theta^2 \pm 2\sqrt{X_\mp} \sqrt{P_\odot} \theta \cos(\pm\Delta_{31} + \delta) + P_\odot. \end{aligned} \quad (\text{A1})$$

The coefficients P_\odot and X_\pm are simply

$$\begin{aligned} \sqrt{P_\odot} &= \cos \theta_{23} \sin 2\theta_{12} \frac{\sin(aL)}{(aL)} \Delta_{21}, \\ \sqrt{X_\pm} &= 2 \sin \theta_{23} \frac{\sin(\pm\Delta_{31} - aL)}{(\pm\Delta_{31} - aL)} \Delta_{31}, \end{aligned}$$

where $\Delta_{ij} = |\delta m_{ij}^2|L/4E$ and $a = G_F N_e / \sqrt{2} \approx (4000 \text{ km})^{-1}$. The atmospheric amplitude for $\nu_\mu \rightarrow \nu_e$ is $\pm\sqrt{X_\pm}\theta$ whereas the solar amplitude is $\sqrt{P_\odot}$ and the relative phase between these two amplitudes⁵ is $(\pm\Delta_{31} + \delta)$. In vacuum, $X_+ = X_- \equiv X_0$ and the two probabilities are identical, as they must since they are CPT conjugates.

⁵ The full amplitude for $\nu_\mu \rightarrow \nu_e$ is $(\pm\sqrt{X_\pm}\theta e^{-i(\pm\Delta_{31}+\delta)} + \sqrt{P_\odot})$.

The other related CPT conjugate pair of appearance probabilities, $P(\nu_e \rightarrow \nu_\mu)$ and $\bar{P}(\bar{\nu}_\mu \rightarrow \bar{\nu}_e)$, can be obtained from the above by changing the sign of δ , as follows

$$\begin{aligned} P(\nu_e \rightarrow \nu_\mu) &= X_\pm \theta^2 \pm 2\sqrt{X_\pm} \sqrt{P_\odot} \theta \cos(\pm\Delta_{31} - \delta) + P_\odot \\ \bar{P}(\bar{\nu}_e \rightarrow \bar{\nu}_\mu) &= X_\mp \theta^2 \pm 2\sqrt{X_\mp} \sqrt{P_\odot} \theta \cos(\pm\Delta_{31} - \delta) + P_\odot. \end{aligned} \quad (\text{A2})$$

The difference between the first two CPT conjugate appearance probabilities, is given by

$$P(\nu_\mu \rightarrow \nu_e) - \bar{P}(\bar{\nu}_e \rightarrow \bar{\nu}_\mu) = \pm\theta (\sqrt{X_+} - \sqrt{X_-}) \left[(\sqrt{X_+} + \sqrt{X_-})\theta \pm 2\sqrt{P_\odot} \cos(\pm\Delta_{13} + \delta) \right].$$

This quantity is positive for the normal hierarchy (NH) and negative for the inverted hierarchy (IH), if

$$\sqrt{X_+} > \sqrt{X_-} \quad \text{and} \quad \theta > 2\sqrt{P_\odot}/(\sqrt{X_+} + \sqrt{X_-}) \approx \sqrt{P_\odot}/\sqrt{X_0}, \quad (\text{A3})$$

for all values of the CP phase δ . The constraint on θ requires⁶

$$\sin^2 2\theta_{13} > \frac{\sin^2 2\theta_{12} \Delta_{21}^2}{\tan^2 \theta_{23} \sin^2 \Delta_{31}} \sim 0.001 - 0.002, \quad (\text{A4})$$

whereas the constraint, $\sqrt{X_+} > \sqrt{X_-}$, is satisfied near the first oscillation maximum provided $(aL) \ll 1$, i.e. $L \ll 4000 \text{ km}$.

With these rather weak constraints then

$$P(\nu_\mu \rightarrow \nu_e) > \bar{P}(\bar{\nu}_e \rightarrow \bar{\nu}_\mu) \quad \text{for NH} \quad (\text{A5})$$

$$\text{and} \quad P(\nu_\mu \rightarrow \nu_e) < \bar{P}(\bar{\nu}_e \rightarrow \bar{\nu}_\mu) \quad \text{for IH} \quad (\text{A6})$$

for all values of the CP phase δ . For the normal (inverted) hierarchy, the matter effect enhances (suppresses) the $P(\nu_\mu \rightarrow \nu_e)$ channel and suppresses (enhances) the $\bar{P}(\bar{\nu}_e \rightarrow \bar{\nu}_\mu)$ channel, thus the matter effect in a sense is used twice. Of course, the difference between these two appearance probabilities is larger at larger values of θ and at larger values of the matter effect. This is the effect that is exploited here to determine the neutrino mass hierarchy.

In the $P(\nu_\mu \rightarrow \nu_e)$ versus $\bar{P}(\bar{\nu}_e \rightarrow \bar{\nu}_\mu)$ plane the trajectory for fixed value of θ as the CP phase δ is varied from 0 to 2π is in general an ellipse which collapses to a line if the E/L of both channels is the same. The centre of this ellipse is given by

$$(\bar{P}(\bar{\nu}_e \rightarrow \bar{\nu}_\mu), P(\nu_\mu \rightarrow \nu_e)) = (X_\mp \theta^2 + P_\odot, X_\pm \theta^2 + P_\odot). \quad (\text{A7})$$

⁶ This is the value of θ at which the atmospheric and solar amplitudes have the same magnitude in vacuum.

Thus, as θ is varied, the centre of the ellipses form lines with slope given by

$$\begin{aligned} \alpha_+ &\equiv \frac{X_-}{X_+} \quad \text{for NH} \\ \text{and } \alpha_- &\equiv \frac{X_+}{X_-} \quad \text{for IH.} \end{aligned} \tag{A8}$$

If the matter effect is small, $(aL) \ll \Delta_{31}$, one can perform a Taylor series about the vacuum such that

$$\alpha_{\pm} = 1 \mp 4(aL)[\Delta_{31}^{-1} - \cot \Delta_{31}] + \mathcal{O}(aL)^2. \tag{A9}$$

It is the difference in the slopes of the two lines (for the normal hierarchy, α_+ and for the inverted hierarchy, α_-) which provides the separation between the allowed regions for two hierarchies in the $P(\nu_\mu \rightarrow \nu_e)$ versus $\overline{P}(\bar{\nu}_e \rightarrow \bar{\nu}_\mu)$ plane.

-
- [1] B. T. Cleveland *et al.*, *Astrophys. J.* **496**, 505 (1998); Y. Fukuda *et al.* [Kamiokande Collaboration], *Phys. Rev. Lett.* **77**, 1683 (1996); J. N. Abdurashitov *et al.* [SAGE Collaboration], *J. Exp. Theor. Phys.* **95**, 181 (2002); W. Hampel *et al.* [GALLEX Collaboration], *Phys. Lett. B* **447**, 127 (1999); T. A. Kirsten [GNO Collaboration], *Nucl. Phys. Proc. Suppl.* **118**, 33 (2003).
 - [2] S. Fukuda *et al.* [Super-Kamiokande Collaboration], *Phys. Lett. B* **539**, 179 (2002).
 - [3] Q. R. Ahmad *et al.* [SNO Collaboration], *Phys. Rev. Lett.* **87**, 071301 (2001).
 - [4] Q. R. Ahmad *et al.* [SNO Collaboration], *Phys. Rev. Lett.* **89**, 011301 (2002) and *ibid.* **89**, 011302 (2002).
 - [5] S. N. Ahmed *et al.* [SNO Collaboration], *Phys. Rev. Lett.* **92**, 181301 (2004).
 - [6] B. Aharmim *et al.* [SNO Collaboration], *Phys. Rev. C* **72**, 055502 (2005).
 - [7] Y. Ashie *et al.* [Super-Kamiokande Collaboration], *Phys. Rev. D* **71**, 112005 (2005).
 - [8] K. Eguchi *et al.* [KamLAND Collaboration], *Phys. Rev. Lett.* **90**, 021802 (2003).
 - [9] M. H. Ahn *et al.* [K2K Collaboration], *Phys. Rev. D* **74**, 072003 (2006).
 - [10] E. Ables *et al.* [MINOS Collaboration], FERMILAB-PROPOSAL-0875.
 - [11] D. G. Michael *et al.* [MINOS Collaboration], *Phys. Rev. Lett.* **97**, 191801 (2006).
 - [12] B. Pontecorvo, *Sov. Phys. JETP* **6**, 429 (1957) [*Zh. Eksp. Teor. Fiz.* **33**, 549 (1957)] and *ibid.* **7**, 172 (1958) [*ibid.* **34** (1958) 247]; Z. Maki, M. Nakagawa and S. Sakata, *Prog. Theor. Phys.* **28**, 870 (1962).

- [13] M. Apollonio *et al.* [CHOOZ Collaboration], Phys. Lett. B **466**, 415 (1999).
- [14] F. Boehm *et al.*, Phys. Rev. Lett. **84**, 3764 (2000) and Phys. Rev. D **62**, 072002 (2000).
- [15] M. C. Gonzalez-Garcia and M. Maltoni, arXiv:0704.1800 [hep-ph].
- [16] T. Araki *et al.* [KamLAND Collaboration], Phys. Rev. Lett. **94**, 081801 (2005).
- [17] L. Wolfenstein, Phys. Rev. D **17**, 2369 (1978); V. D. Barger, K. Whisnant, S. Pakvasa and R. J. N. Phillips, Phys. Rev. D **22**, 2718 (1980); S. P. Mikheev and A. Y. Smirnov, Sov. J. Nucl. Phys. **42**, 913 (1985); S. J. Parke, Phys. Rev. Lett. **57**, 1275 (1986); H. W. Zaglauer and K. H. Schwarzer, Z. Phys. C **40**, 273 (1988); M. C. Banuls, G. Barenboim and J. Bernabeu, Phys. Lett. B **513**, 391 (2001); M. Freund *et al.*, Nucl. Phys. B **578**, 27 (2000).
- [18] J. Arafune, M. Koike and J. Sato, Phys. Rev. D **56**, 3093 (1997) [Erratum-ibid. D **60**, 119905 (1999)]; H. Minakata and H. Nunokawa, Phys. Lett. B **413**, 369 (1997); A. Donini *et al.*, Nucl. Phys. B **574**, 23 (2000).
- [19] H. Minakata, H. Nunokawa and S. J. Parke, Phys. Rev. D **68**, 013010 (2003).
- [20] A. de Bellefon *et al.*, arXiv:hep-ex/0607026; J. E. Campagne, M. Maltoni, M. Mezzetto and T. Schwetz, JHEP **0704**, 003 (2007); T. Schwetz, JHEP **0705**, 093 (2007).
- [21] D. S. Ayres *et al.* [NOvA Collaboration], hep-ex/0503053. FERMILAB-PROPOSAL-0929, March 21, 2005. Revised NO ν A Proposal available at http://www-nova.fnal.gov/NOvA_Proposal/Revised_NOvA_Proposal.html
- [22] A. Para and M. Szleper, hep-ex/0110032.
- [23] P. Zucchelli, Phys. Lett. B **532**, 166 (2002).
- [24] M. Mezzetto, J. Phys. G **29**, 1771 (2003).
- [25] J. Burguet-Castell *et al.*, Nucl. Phys. B **695**, 217 (2004);
- [26] C. H. Albright *et al.*, arXiv:physics/0411123; J. Burguet-Castell *et al.*, Nucl. Phys. B **725**, 306 (2005). P. Huber *et al.*, Phys. Rev. D **73**, 053002 (2006); A. Donini and E. Fernandez-Martinez, Phys. Lett. B **641**, 432 (2006); A. Donini *et al.*, Eur. Phys. J. C **48**, 787 (2006); A. Blondel *et al.*, Acta Phys. Polon. B **37**, 2077 (2006); S. K. Agarwalla, S. Choubey and A. Raychaudhuri, Nucl. Phys. B **771**, 1 (2007); S. K. Agarwalla *et al.*, Phys. Rev. D **75**, 097302 (2007); A. Donini *et al.*, arXiv:hep-ph/0703209.
- [27] ISS Working Group, arXiv:0710.4947v1 [hep-ph].
- [28] H. Minakata and H. Nunokawa, JHEP **0110**, 001 (2001).
- [29] O. Mena, H. Nunokawa and S. J. Parke, Phys. Rev. D **75**, 033002 (2007)

- [30] O. Mena, arXiv:hep-ph/0609031.
- [31] P. Huber, M. Lindner and W. Winter, Nucl. Phys. B **654**, 3 (2003).
- [32] V. Barger, D. Marfatia and K. Whisnant, Phys. Lett. B **560**, 75 (2003).
- [33] O. Mena Requejo, S. Palomares-Ruiz and S. Pascoli, Phys. Rev. D **72**, 053002 (2005).
- [34] O. Mena, S. Palomares-Ruiz and S. Pascoli, Phys. Rev. D **73**, 073007 (2006).
- [35] M. Ishitsuka *et al.*, Phys. Rev. D **72**, 033003 (2005); K. Hagiwara, N. Okamura and K. i. Senda, Phys. Lett. B **637**, 266 (2006).
- [36] Y. Hayato *et al.*, Letter of Intent, available at <http://neutrino.kek.jp/jhfnu/>
- [37] <http://cern.ch/beta-beam>
- [38] C. Rubbia *et al.*, Nucl. Instrum. Meth. A **568**, 475 (2006). [arXiv:hep-ph/0602032].
- [39] A. Blake, private communication.